King Saud University

Arabian Journal of Chemistry

www.ksu.edu.sa
www.sciencedirect.com

ORIGINAL ARTICLE

Computational insights into quinoxaline-based corrosion inhibitors of steel in HCl: Quantum chemical analysis and QSPR-ANN studies

Taiwo W. Quadri [a], Lukman O. Olasunkanmi [b,c], Omolola E. Fayemi [a], Hassane Lgaz [d,*], Omar Dagdag [e], El-Sayed M. Sherif [f], Awad A. Alrashdi [g], Ekemini D. Akpan [e], Han-Seung Lee [h,*], Eno E. Ebenso [e,*]

[a] *Department of Chemistry, School of Chemical and Physical Sciences and Material Science Innovation & Modelling (MaSIM) Research Focus Area, Faculty of Natural and Agricultural Sciences, North-West University, Private Bag X2046, Mmabatho 2735, South Africa*
[b] *Department of Chemistry, Faculty of Science, Obafemi Awolowo University, Ile Ife 220005, Nigeria*
[c] *Department of Chemical Sciences, University of Johannesburg, P.O. Box 17011, Doornfontein Campus, Johannesburg 2028, South Africa*
[d] *Innovative Durable Building and Infrastructure Research Center, Center for Creative Convergence Education, Hanyang University-ERICA, 55 Hanyangdaehak-ro, Sangrok-gu, Ansan-si, Gyeonggi-do, 15588, Korea*
[e] *Institute for Nanotechnology and Water Sustainability, College of Science, Engineering and Technology, University of South Africa, Johannesburg 1710, South Africa*
[f] *Department of Mechanical Engineering, College of Engineering, King Saud University, P.O. Box 800, Al-Riyadh 11421, Saudi Arabia*
[g] *Chemistry Department, Umm Al-Qura University, Al-Qunfudah University College, Saudi Arabia*
[h] *Department of Architectural Engineering, Hanyang University-ERICA, 1271 Sa 3-dong, Sangrok-gu, Ansan 426791, Korea*

Abstract The inhibition of mild steel deterioration via organic substances has become popular nowadays. Among the myriads of organic substances applied as potential inhibitors, quinoxalines stand out as toxic-free, cheap and effective compounds in different electrolytes. This report investigates the computational aspects of selected quinoxaline compounds tested as suppressors of mild steel deterioration in HCl medium using quantum chemical method (Density Functional Theory, DFT) and quantitative structure property relationship (QSPR). Feature selection tool was utilized

---

* Corresponding authors.
  E-mail addresses: hlgaz@hanyang.ac.kr (H. Lgaz), ercleehs@hanyang.ac.kr (H.-S. Lee), ebensee@unisa.ac.za (E.E. Ebenso).
Peer review under responsibility of King Saud University.

Production and hosting by Elsevier

Ordinary least squares
regression;
Artificial neural network

to choose five top molecular descriptors (constitutional indices) that were used to characterize the quinoxaline molecules. Linear (ordinary least squares regression) and nonlinear (artificial neural network) modelling were adopted to correlate the selected constitutional indices of the studied quinoxalines with their experimental inhibition performances. The nonlinear model showed better performance as shown by the obtained results; RMSE of 5.4160, MSE of 29.3336, MAD of 2.3816 and MAPE of 5.0389. The developed models were utilized to determine the inhibition performances of ten new quinoxaline-based corrosion inhibitors which showed excellent inhibition performances of 87.88 to 95.73%.

1. Introduction

Metallic deterioration has received a lot of attention in the academic and research communities because of its socio-economic effects on the world at large (Saranya et al., 2021). The economic impact of corrosion has been reported to be 3–5% of the annual global gross domestic product (GDP) which amounts to nearly \$2.5 trillion (Mishra et al., 2018). Corrosion has direct effect on materials that humans heavily depend upon for survival and convenience. More so, corrosion has resulted in the collapse of bridges and buildings as well as contamination of water bodies due to pipe bursts/explosions which affect human and aquatic life (Goni and Mazumder, 2019). Chemical inhibitors have been widely formulated by corrosion researchers to mitigate metallic corrosion. Quinoxalines belong to a group of organic inhibitors that have been widely assessed for their inhibitive properties in different corrosive media (Chauhan et al., 2020, Saranya et al., 2021). They have also been found to be environmentally friendly and suited for application in various chemical, mechanical, material and metallurgical industries. The high performance of quinoxaline-based corrosion inhibitors has been traced to the functional groups, conjugate multiple bonds and aromatic rings present in their molecular structures. Generally, researchers have employed theoretical tools such as quantum chemical studies and atomic simulations to identify relevant electronic and structural properties that relate to the inhibition performance. Moreover, several studies have applied results from theoretical calculations such as density functional theory (DFT) and molecular simulations to interpret the inhibition mechanism of investigated quinoxalines (Zarrouk et al., 2013, Zarrouk et al., 2014, Ouakki et al., 2021).

Quantitative structure property relationship (QSPR) is the one of the latest and reliable theoretical methods that has been widely used in designing drugs and developing new materials for different applications (Liu et al., 2017, Lin et al., 2020). This technique makes it possible to forecast the property of interest for a series of non-tested compounds based on the established relationship between the differences in their structural features and the targeted property (Al-Fakih et al., 2016, Rybińska-Fryca et al., 2020). QSPR has become a desirable approach for determining the inhibition performance of potential chemical compounds. The process of QSPR analysis begins with collection and preparation of inhibitor molecules and their experimental inhibition efficiencies (IE%). Thousands of molecular descriptors comprising electronic and structural descriptors derived from calculations performed using theoretical software packages are reduced to a relevant small number. Selection of relevant molecular descriptors utilized in model development is often done using feature selection tools. As a rule of thumb, Topliss and Costello proposed that the ratio of chemical compounds to molecular descriptors should be at least 5:1 for simple linear models to avoid overfitting (Topliss and Costello, 1972, Topliss and Edwards, 1979). The selected relevant molecular descriptors are utilized in developing correlation models via linear and/or nonlinear methods which are validated using statistical indicators and further employed in designing novel organic inhibitors (Quadri et al., 2021b). Molecular descriptors are the most significant and critical elements in obtaining a reliable QSPR model as they are employed

in modelling several different chemical properties in scientific fields (Khan, 2016). The type of molecular descriptors employed and how best they encode the structural features of chemical compounds that are correlated to the activity are critical determinants of the reliability of any QSPR model. An ideal descriptor is expected to be related to a wide range of compounds, correlate with the structural characteristics for inhibition performance, show insignificant correlation with other descriptors and should be easily computed. Additionally, an ideal descriptor should yield different values for molecules with different structures and should possess physical interpretation (Puzyn et al., 2010, Roy et al., 2015a,b).

Instances of QSPR models developed to study the relationship between features of organic compounds and IE% include a study conducted by Zhao and coworkers (Zhao et al., 2014). They performed quantum chemical studies and molecular dynamic simulations on 19 amino acids tested as anticorrosive agents for mild steel degradation in hydrochloric acid. Subsequently, feature selection of obtained chemical descriptors was done using principal component analysis (PCA) before QSPR model building. The model was constructed using a nonlinear technique, support vector machine (SVM) and the model performance was determined by the root mean square error (RMSE) and correlation coefficient (R^2) value. Individual quantum chemical indices were correlated with the IE% and showed low correlation which necessitated the demand for a nonlinear model. Reported statistical parameters for RMSE and R^2 were 1.48 and 0.97 for the testing set which showed good performance. The authors theoretically designed 5 amino acids and the predicted IE% was in the range of 62 to 68%. In another study, this research group reported theoretical approaches of DFT calculations and molecular simulations to study the inhibitive properties of 20 benzimidazole-based inhibitors (Li et al., 2015). Correlation of molecular descriptors with IE% conducted with a linear model generally showed poor results, improved results were obtained when descriptors for protonated forms of the benzimidazoles were used. PCA was conducted to select appropriate quantum chemical parameters to be considered for modelling. Nonlinear SVM was adopted to develop the QSPR model for the studied benzimidazoles using six DFT-based indices of the protonated organic inhibitors including nuclear independent chemical shift (NICS). The reliability and predictive power of the model was demonstrated by the obtained results; low RMSE (6.79) and high R^2 (0.96). The established model was adopted to calculate 6 newly designed benzimidazole molecules. Al-Fakih and coworkers built a QSPR model for 18 furan derivatives previously tested to impede metallic disintegration in HCl. Dragon 6 was used to calculate over 4,000 chemical descriptors that were reduced to 12 useful variables using the sure independence screening method (Al-Fakih et al., 2016). Two stage sparse multiple linear regression (MLR) was conducted, and the obtained results showed that the elastic net method yielded a better predictive capacity than the ridge penalty model judging by the two statistical criteria used (MSE and R^2). In another study, seven DFT-based parameters were derived from 11 thiophene molecules used as chemical additives for metallic corrosion inhibition. The authors developed a neural network model to corre-

late the selected molecular variables with the experimental IE% and obtained an excellent correlation of 0.958 which indicated the predictive potential of the developed model (Khaled and Al-Mobarak, 2012).

The aim of the present report is to present computational insight into the inhibition mechanism of 40 quinoxalines using quantum chemical method and QSPR model with constitutional indices as input parameters. Quantum chemical parameters are commonly used as input variables for QSPR model construction but recently, some researchers have continued to challenge the simplistic correlation often reported between quantum chemical indices and inhibition performances (Kokalj, 2010, Winkler et al., 2014, Winkler et al., 2016, Kokalj, 2021, Kokalj et al., 2021). Constitutional indices derived from Dragon 7 software have been employed in this study to model the relationship between experimental inhibition performances and 40 quinoxaline molecules. Linear model using ordinary least squares regression (OLS) and nonlinear model via artificial neural network (ANN) was developed. Several studies have reported traditional linear regression tools in QSPR model development. On the other hand, ANN which offers a modern intelligent approach to solving regression and classification problems has been scarcely reported. ANN has gained wide acceptance and applications in several fields of study and is also suitable for QSPR studies in corrosion inhibition. Furthermore, the built models were used to forecast the inhibition performances of 10 non-synthesized, non-tested quinoxaline molecules as potential inhibitors of metallic deterioration in acidic solution.

2. Materials and methods

2.1. Selected quinoxaline compounds

A database of 40 quinoxaline-based corrosion inhibitors and their inhibition performances were retrieved from published reports (Adardour et al., 2010, Benbouya et al., 2012, Fu et al., 2012, Adardour et al., 2013, El-Hajjaji et al., 2014, Olasunkanmi et al., 2015, Lgaz et al., 2016a,b, Olasunkanmi et al., 2016a,b, Tazouti et al., 2016, Rbaa et al., 2018, Benhiba et al., 2020, Laabaissi et al., 2020, Olasunkanmi and Ebenso, 2020). Data curation and filtration were done to ensure the development of a reliable model. This includes ensuring collected data are from reliable sources, confirming the correctness of the molecular structures of collected compounds, and removing redundant and/or duplicate inhibitor molecules if any (Golbraikh et al., 2012). Important information on the collected series of quinoxalines used for QSPR model development are displayed in Table 1. From the table, it is clear that 4-(quinoxalin-2-yl)phenol (PHQX) offered the maximum protection of 98.30% to the steel substrate.

2.2. Molecular descriptors calculation

The study considered molecular descriptors derived from quantum chemical calculations and Dragon 7 software. Quantum chemical descriptors were generated by carrying out DFT calculations using B3LYP functional with 6-31 + (d,p) basis set on the neutral forms of the quinoxaline molecules in aqueous and gaseous phases.The chemical structures of the quinoxalines were modelled using ChemDraw Professional 15.0 software and viewed using Gaussview 5.0. Optimizations of the molecules to a local minimum were performed using Gaussian 09 software and full optimization was verified by the absence of imaginary vibrational frequencies. Total energy (TE), dipole moment (μ) and energies of the lowest unoccupied molecular

orbital (E_{LUMO}) and highest occupied molecular orbital (E_{HOMO}) were obtained for all the studied molecules. Other molecular descriptors for the inhibitor molecules were calculated using the following equations (Yusuf et al., 2020, Quadri et al., 2021a).

$$\Delta E = E_{LUMO} - E_{HOMO} \tag{1}$$

$$EA = -E_{LUMO} \tag{2}$$

$$IP = -E_{HOMO} \tag{3}$$

$$\chi = -\frac{1}{2}(E_{HOMO} + E_{LUMO}) \tag{4}$$

$$\eta = \frac{1}{2}(E_{LUMO} - E_{HOMO}) \tag{5}$$

$$\sigma = \eta^{-1} \tag{6}$$

$$\Delta N = \frac{\chi_{Fe} - \chi_{inh}}{2(\eta_{Fe} + \eta_{inh})} \tag{7}$$

where ΔE, EA, IP, χ, η, σ and ΔN represent energy gap, electron affinity, ionization potential, absolute electronegativity, global hardness, global softness and change in the number of electrons transferred, respectively.
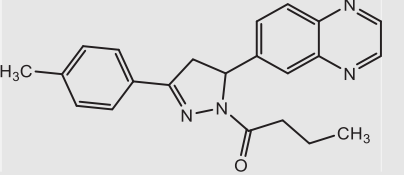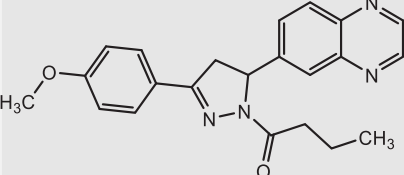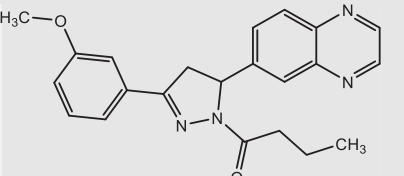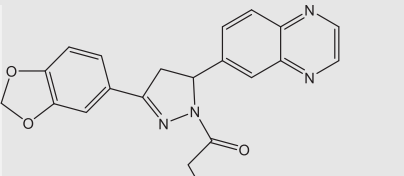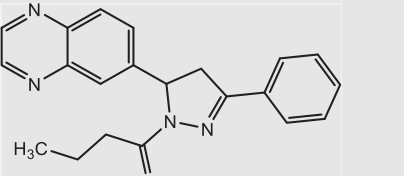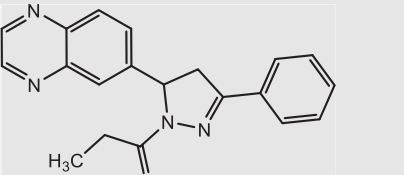
Using the optimized molecular structures, numerous molecular descriptors were obtained from Dragon 7 (Mauri et al., 2006). Dragon 7 is a software application that calculates above 5000 molecular descriptors (0D, 1D, 2D and 3D) divided into 30 categories which can be used for QSPR modelling. Optimized quinoxaline molecules were converted from .log to .mdl file format using Open Babel (O'Boyle et al., 2011) and were used as inputs into Dragon 7 to calculate a host of molecular descriptors. Preliminary eliminations of high dimensional descriptors were done using the Dragon 7 software to remove descriptors with missing entries, descriptors with zero values and those with constant and/or near constant values. In addition, multicollinear descriptors and descriptors having standard deviation (SD) lower than 0.0001 were removed. The filtered descriptors were combined with DFT-based descriptors and subjected to standardization with the aim of ranking the descriptors in order of relative significance to the experimental IE%. This process was performed using Minitab 7.

2.3. Statistical modelling

Ordinary least squares regression, a form of MLR, was utilized to model the linear correlation between the filtered chemical variables (X) and the inhibition performance (Y) where X denotes the independent variable and Y is the dependent variable. The OLS regression was carried out using Minitab 7 and characterized by correlation coefficient and standard deviation.

On the other hand, ANN was adopted to model the nonlinear relationship between the chosen chemical variables and the inhibition performances of the investigated 40 quinoxaline molecules. Using a supervised learning method and a feedforward backpropagation architecture, neural network modelling was performed using Matlab. Six input parameters comprising five selected constitutional indices and inhibitor concentration served as the inputs, while three hidden neurons governed by logsig activation function and five hidden neurons controlled

Table 1 Molecular structures and experimental IE% of the investigated quinoxaline-based corrosion inhibitors.
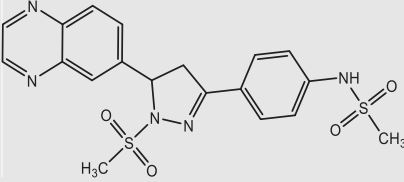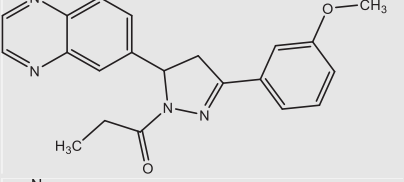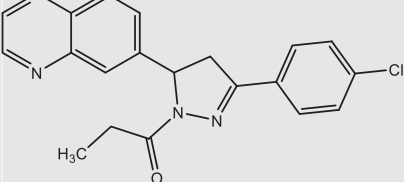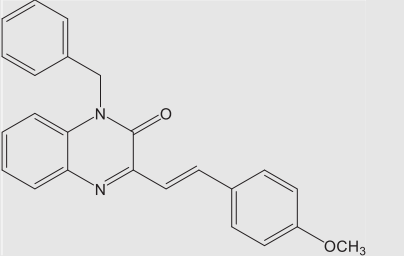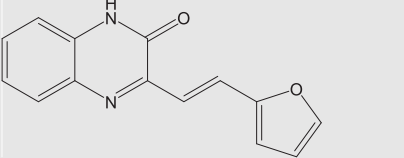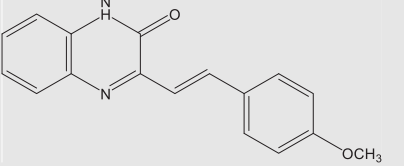
S/N	Quinoxalines	Chemical structures	IE%	Ref
1.	1-[3-(4-methylphenyl)-5-(quinoxalin-6-yl)-4,5-dihydropyrazol-1-yl]butan-1-one (Me-4-PQPB)		80.42	Olasunkanmi et al. (2016a)
2.	1-[3-(4-methoxyphenyl)-5-(quinoxalin-6-yl)-4,5-dihydro-1H-pyrazol-1-yl]butan-1-one (Mt-4-PQPB)		72.01	Olasunkanmi et al. (2016a)
3.	1-[3-(3-methoxylphenyl)-5-(quinoxalin-6-yl)-4,5-dihydropyrazol-1-yl]butan-1-one (Mt-3-PQPB)		69.66	Olasunkanmi et al. (2016a)
4.	1-[3-(2H-1,3-benzodioxol-5-yl)-5-(quinoxalin-6-yl)-4,5-dihydropyrazol-1-yl]butan-1-one (Oxo-PQPB)		68.41	Olasunkanmi et al. (2016a)
5.	1-[3-(phenyl-5-quinoxalin-6-yl)-4,5-dihydro-1H-pyrazol-1-yl]butan-1-one (PQDPB)		90.50	Olasunkanmi et al. (2015)
6.	1-[3-(phenyl-5-quinoxalin-6-yl)-4,5-dihydro-1H-pyrazol-1-yl]propan-1-one (PQDPP)		93.65	Olasunkanmi et al. (2015)

Table 1 (*continued*)
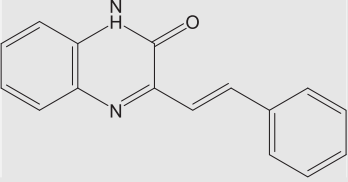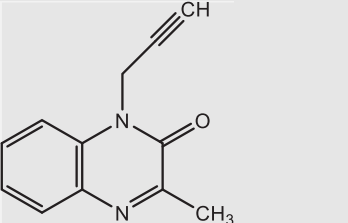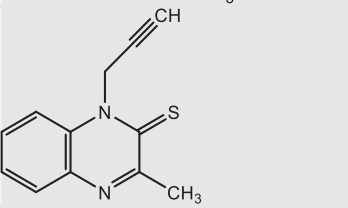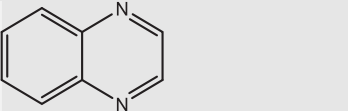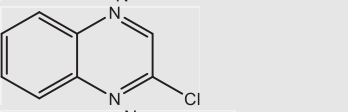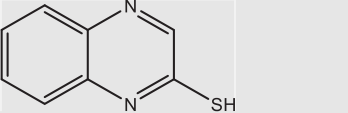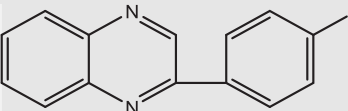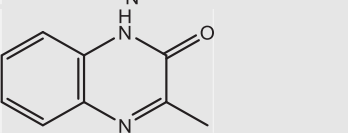
S/N	Quinoxalines	Chemical structures	IE%	Ref
7.	2-phenyl-1-[3-phenyl-5-(quinoxalin-6-yl)-4,5-dihydro-1H-pyrazol-1-yl]ethanone (PPQDPE)		86.88	Olasunkanmi et al. (2015)
8.	N-{2-[1-propanoyl-5-(quinoxalin-6-yl)-4,5-dihydro-1H-pyrazol-3-yl]phenyl} methanesulfonamide (MS-2-PQPP)		91.54	Olasunkanmi et al. (2016b)
9.	N-{3-[1-propanoyl-5-(quinoxalin-6-yl)-4,5-dihydro-1H-pyrazol-3-yl]phenyl} methanesulfonamide (MS-3-PQPP)		93.88	Olasunkanmi et al. (2016b)
10.	N-{4-[1-propanoyl-5-(quinoxalin-6-yl)-4,5-dihydropyrazol-3-yl]phenyl} methanesulfonamide (MS-4-PQPP)		93.56	Olasunkanmi et al. (2016b)
11.	N-{2-[1-(methanesulfonyl)-5-(quinoxalin-6-yl)-4,5-dihydro-1H-pyrazol-3-yl] phenyl}methanesulfonamide (MS-2-PQPMS)		92.68	Olasunkanmi et al. (2016b)
12.	N-{3-[1-(methanesulfonyl)-5-(quinoxalin-6-yl)-4,5-dihydro-1H-pyrazol-3-yl] phenyl}methanesulfonamide (MS-3-PQPMS)		93.39	Olasunkanmi et al. (2016b)

S/N	Quinoxalines	Chemical structures	IE%	Ref
13.	N-{4-[1-(methanesulfonyl)-5-(quinoxalin-6-yl)-4,5-dihydro-1H-pyrazol-3-yl]phenyl}methanesulfonamide (MS-4-PQPMS)		94.00	Olasunkanmi et al. (2016b)
14.	1-[3-(3-methoxyphenyl)-5-(quinoxalin-6-yl)-4,5-dihydropyrazol-1-yl]propan-1-one (Mt-3-PQPP)		93.69	Olasunkanmi and Ebenso (2020)
15.	1-(3-(4-chlorophenyl)-5-(quinoxalin-6-yl)-4,5-dihydro-1H-pyrazol-1-yl)propan-1-one (Cl-4-PQPP)		92.27	Olasunkanmi and Ebenso (2020)
16.	(E)-1-benzyl-3-(4-methoxystyryl)quinoxalin-2(1H)-one (QN1)		93.00	Lgaz et al. (2016a)
17.	(E)-3-(2-(furan-2-yl)vinyl)quinoxalin-2(1H)-one (QN2)		90.00	Lgaz et al. (2016a)
18.	(E)-3-(4-methoxystyryl)quinoxalin-2(1H)-one (QN3)		87.00	Lgaz et al. (2016a)

Table 1 (*continued*)

S/N	Quinoxalines	Chemical structures	IE%	Ref
19.	(E)-3-styrylquinoxalin-2(1H)-one (QN4)		85.00	Lgaz et al. (2016a)
20.	3-methyl-1-prop-2-ynylquinoxalin-2(1H)-one (Pr-N-Q = O)		88.80	El-Hajjaji et al. (2014)
21.	3-methyl-1-prop-2-ynylquinoxaline-2 (1H)-thione (Pr-N-Q = S)		92.30	El-Hajjaji et al. (2014)
22.	Quinoxaline (QX)		84.20	Fu et al. (2012)
23.	2-chloroquinoxaline (CHQX)		92.50	Fu et al. (2012)
24.	2-quinoxalinethiol (THQX)		95.50	Fu et al. (2012)
25.	4-(quinoxalin-2-yl)phenol (PHQX)		98.30	Fu et al. (2012)
26.	3-methylquinoxalin-2(1H)-one (Q = O)		66.60	Benbouya et al. (2012)

Table 1 (*continued*)

S/N	Quinoxalines	Chemical structures	IE%	Ref
27.	3-methylquinoxalin-2(1H)-thione (Q = S)		82.80	Benbouya et al. (2012)
28.	7-chloro-3-methylquinoxalin-2(1H)-thione (Cl-Q = S)		75.00	Benbouya et al. (2012)
29.	7-chloro-2-(4-methoxyphenyl)thieno[2,3-b]quinoxaline (CMOPTQ)		89.00	Adardour et al. (2013)
30.	7-chloro-3-(4-methoxystyryl)quinoxalin-2-one (CMOSQ)		87.00	Adardour et al. (2013)
31.	(E)-3-(4-methoxystyryl)-7-methylquinoxalin-2(1H)-one (MOSMQ)		92.00	Tazouti et al. (2016)
32.	(E)-3-(2-(furan-2-yl)vinyl) quinoxalin2(1H)-one (FVQ)		94.98	Lgaz et al. (2016b)
33.	3,7-dimethylquinoxalin-2 (1H)-one (DMQ = O)		88.07	Adardour et al. (2010)
34.	3,7-dimethylquinoxalin-2 (1H)-thione (DMQ = S)		93.27	Adardour et al. (2010)

Table 1 (*continued*)

S/N	Quinoxalines	Chemical structures	IE%	Ref
35.	1,4-bis((8-hydroxyquinolin-5-yl)-methyl)-6-methylquinoxalin-2,3-(1H,4H)-dione (Q-HNHyQ)		89.40	Rbaa et al. (2018)
36.	1,4-bis-((8-hydroxyquinolin-5-yl)-methyl)-quinoxalin-2,3-(1H,4H)-dione (QCH3NHyQ)		95.40	Rbaa et al. (2018)
37.	2-(2,4-dichlorophenyl)-1,4-dihydroquinoxaline (HQ)		91.00	Benhiba et al., (2020)
38.	2-(2,4-dichlorophenyl)-6-methyl-1,4-dihydroquinoxaline (CQ)		94.20	Benhiba et al., (2020)
39.	(E)-3-(4-chlorostyryl)quinoxalin-2(1H)-one (CSQN)		92.80	Laabaissi et al. (2020)
40.	(E)-3-(4-(dimethylamino)styryl)quinoxalin-2(1H)-one (NSQN)		96.40	Laabaissi et al. (2020)

by the softmax activation function were utilized to model the output inhibition efficiencies (Fig. 1). The Levenberg-Marquardt training algorithm was implemented because of its effectiveness and quick convergence. Several iterations (training and retraining) were carried out until a low statistical error value was obtained.

2.4. Statistical criteria

The performance of the linear model was characterized using R^2 and SD while the nonlinear model was characterized using several statistical criteria. Statistically robust and reliable models are demonstrated by low statistical error values. The main statistical parameters are obtained using the following relationships (Gramatica 2013, Eftekhari et al., 2018, Liu et al., 2019, Olatunji et al., 2019, Adedeji et al., 2020a,b):

Root mean square error,

$$RMSE = \sqrt{\frac{\sum_{k=1}^{N} [y_k - \widehat{y_k}]^2}{N}} \tag{8}$$

Mean square error,

$$MSE = \frac{\sum_{k=1}^{N} [y_k - \widehat{y_k}]^2}{N} \tag{9}$$

Mean average deviation,

$$MAD = \frac{1}{N} \sum_{k=1}^{N} |y_k - \bar{y}| \tag{10}$$

Mean average percentage error,

$$MAPE = \frac{1}{N} \sum_{k=1}^{N} \left| \frac{y_k - \widehat{y_k}}{y_k} \right| \times 100\% \tag{11}$$

Coefficient of variation,

Fig. 1   ANN architecture for the model.

$$CoV = \frac{median|\widehat{y_k} - y_{k\_median}|}{y_{k\_median}} \tag{12}$$

Relative mean bias error,

$$rMBE = \frac{1}{N} \sum_{k=1}^{N} \left(\frac{\widehat{y_k} - y_k}{y_k} \right) \tag{13}$$

where N denotes the number of dataset for analyzing each ANN model, y_k, represents the experimental IE%, $\widehat{y_k}$, represents the predicted IE%, y_{k_median} represents the median of the predicted IE% and $\bar{y}$ denotes the mean IE%.

3. Results and discussion

3.1. DFT studies of selected quinoxalines

Inhibition performances of organic corrosion inhibitors of metal are closely correlated with their chemical stability or reactivity. The chemical reactivity of a series of chemical compounds are predicted by the analysis of frontier molecular orbital (FMO) theory. The theory gives useful insight on the probable adsorption centres of the organic molecules under study. From the presented images in Table 2, it is clear that the LUMO and HOMO energy orbitals in aqueous phase are widely spread on the quinoxaline moiety with minimal extension to the different substituent groups in some cases. This indicates that these sites would be the sites of preference for adsorption onto the mild steel (Fu et al., 2012, Olasunkanmi and Ebenso 2020). It should also be noted that there are a few cases where the HOMO and LUMO are localized around the phenyl rings (MS-n-PQPP series) (Olasunkanmi et al., 2016) and a few other cases where nearly all the atoms in the quinoxaline molecule act as sites of adsorption.

Generally, the adherence capacity of inhibitor compounds can be explained as a donor–acceptor interface between the investigated compounds and the metal of interest. E_{HOMO} is proportional to the electron contributing potential of the studied inhibitor, while E_{LUMO} is connected to the electron accepting potential of the investigated compound. Lesser values of energy gap, ΔE are reported to imply higher inhibition efficiencies as these molecules undergo ease of transfer of one or more electrons from the HOMO level to the metallic orbital (Olasunkanmi et al., 2015, Benhiba et al., 2020). Studies have also shown that a hard molecule possesses higher values of energy gap, while the reverse occurs for soft molecules. It is therefore expected that a compound with a greater value of softness and lesser value of hardness will be more reactive and consequently favour adsorption potential ((Lgaz et al., 2016a) (Olasunkanmi et al., 2016a)). Lower TE also indicates that the quinoxaline compound adsorbs favourably through the active adsorption sites (Benhiba et al., 2020). The calculated DFT variables shown in Table 3 for the investigated quinoxalines do not follow any particular trend with respect to the reported experimental IE% due to the complex nature of the reaction occurring at the mild steel/electrolyte interface. The factors affecting the IE% of the quinoxaline-based inhibitors are quite numerous (Li et al., 2015).
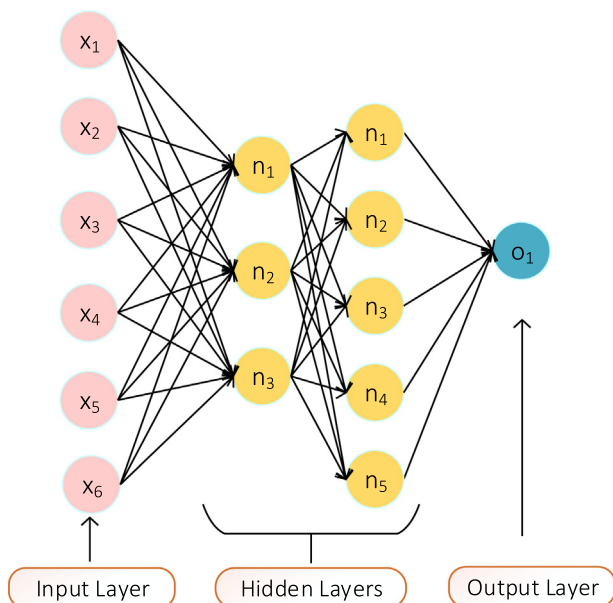
3.2. Feature selection

Few highly informative descriptors from the numerous calculated quantum chemical and Dragon-based descriptors were obtained using feature selection. The MLR standardization method was adopted to carry out feature selection by ranking all the obtained molecular descriptors in order of their standardized coefficients or relative significance. Fig. 2 shows the significant features among the numerous molecular descriptors. The five topmost descriptors shown in Fig. 2 were utilized along with concentration in QSPR analysis using linear modelling (MLR) and nonlinear modelling (ANN) techniques.

The selected descriptors (MW, nCsp2, nCsp3, nO and nN) have been described in Table 4. In addition, the plot of the Pearson's correlation matrix of the selected chemical variables is presented in Table 5.

3.3. MLR model

The obtained mathematical relation representing the QSPR model of investigated quinoxalines using the OLS method is as follows:

Table 2 Molecular orbital electron density distribution for investigated quinoxalines in aqueous phase.

Table 2 (*coninued*)

$$IE(\%) = 74.84 + 270Conc + 0.0440MW + 4.92nN$$
$$- 1.89nO - 4.00nCsp3 - 0.170nCsp2 \qquad (14)$$

$R^2 = 0.3009$, SD $= 7.24607$ where MW, nN, nO, nCsp2 and nCsp3 are the screened descriptors of interest and Conc denotes the concentration of quinoxalines. The developed OLS model clearly showed that the IE% of studied quinoxalines are influenced by increase in Conc, MW, nN and decrease in nO, nCsp3 and nCsp2. The screened descriptors are consti-

tutional indices, which are known to affect the adherence ability of quinoxalines on mild steel surface. Numerous corrosion scientists have investigated the adsorption ability of organic molecules such as quinoxalines with oxygen and nitrogen atoms. These heteroatoms serve as active sites of adsorption thereby offering effective protection for the metal from corrosive ions. In addition, molecules having high molecular weight and sp[2] and sp[3] hybridized carbon atoms have been established to be effective corrosion inhibitors as they serve as anchoring

Table 3 DFT-based indices for neutral forms of quinoxaline molecules in gas and liquid phases, as well as experimental parameters*.

| Quinoxalines	Conc* (M)	Temp* (K)	Phase	TE (eV)	E_{HOMO} (eV)	E_{LUMO} (eV)	ΔE (eV)	μ (D)	IP (eV)	EA (eV)	X (eV)	η (eV)	σ (eV^{-1})	ΔN	IE%*
Me-4-PQPB	0.000280	303	G	−31182.23	−6.035	−2.269	3.766	4.738	6.035	2.269	4.152	1.883	0.531	0.756	**80.42**
			A	−31182.71	−6.143	−2.418	3.725	7.156	6.143	2.418	4.281	1.863	0.537	0.730	
Mt-4-PQPB	0.000270	303	G	−33228.80	−5.839	−2.249	3.590	5.114	5.839	2.249	4.044	1.795	0.557	0.823	**72.01**
			A	−32610.20	−6.160	4.946	11.106	2.632	6.160	−4.946	0.607	5.553	0.180	0.576	
Mt-3-PQPB	0.000270	303	G	−33228.78	−6.077	−2.258	3.819	5.462	6.077	2.258	4.168	1.909	0.524	0.742	**69.66**
			A	−32610.18	−6.523	4.949	11.471	3.332	6.523	−4.949	0.787	5.736	0.174	0.542	
Oxo-PQPB	0.000260	303	G	−34588.63	−6.211	4.910	11.121	2.353	6.211	−4.910	0.650	5.561	0.180	0.571	**68.41**
			A	−35243.16	−5.912	−2.417	3.495	7.146	5.912	2.417	4.165	1.747	0.572	0.811	
PQPDB	0.000170	303	G	−29550.99	−6.574	4.927	11.502	2.529	6.574	−4.927	0.824	5.751	0.174	0.537	**90.50**
			A	−30112.69	−6.256	−2.421	3.835	6.313	6.256	2.421	4.338	1.918	0.521	0.694	
PQDPP	0.000180	303	G	−28501.14	−6.580	4.925	11.505	2.546	6.580	−4.925	0.827	5.753	0.174	0.537	**93.65**
			A	−28501.14	−6.580	4.925	11.505	2.547	6.580	−4.925	0.827	5.753	0.174	0.537	
PPQDPE	0.000150	303	G	−34260.11	−6.202	−2.270	3.932	4.117	6.202	2.270	4.236	1.966	0.509	0.703	**86.88**
			A	−34260.62	−6.296	−2.422	3.874	6.546	6.296	2.422	4.359	1.937	0.516	0.682	
MS-2-PQPP	0.000240	303	G	−46546.65	−6.327	−2.403	3.925	6.173	6.327	2.403	4.365	1.962	0.510	0.671	**91.54**
			A	−46547.39	−6.325	−2.437	3.888	9.869	6.325	2.437	4.381	1.944	0.514	0.674	
MS-3-PQPP	0.000240	303	G	−45739.13	−6.739	4.869	11.608	5.577	6.739	−4.869	0.935	5.804	0.172	0.522	**93.88**
			A	−31560.33	−6.527	4.947	11.474	3.342	6.527	−4.947	0.790	5.737	0.174	0.541	
MS-4-PQPP	0.000240	303	G	−45739.16	−6.470	4.844	11.314	4.062	6.470	−4.844	0.813	5.657	0.177	0.547	**93.56**
			A	−46547.38	−6.118	−2.422	3.695	7.497	6.118	2.422	4.270	1.848	0.541	0.739	
MS-2-PQPMS	0.000230	303	G	−57319.91	−6.589	−2.420	4.169	9.081	6.589	2.420	4.505	2.085	0.480	0.598	**92.68**
			A	−57320.90	−6.471	−2.448	4.023	14.915	6.471	2.448	4.460	2.012	0.497	0.631	
MS-3-PQPMS	0.000230	303	G	−56372.15	−7.070	4.861	11.931	4.737	7.070	−4.861	1.105	5.966	0.168	0.494	**93.39**
			A	−45739.13	−6.739	4.869	11.608	5.577	6.739	−4.869	0.935	5.804	0.172	0.522	
MS-4-PQPMS	0.000230	303	G	−57319.87	−6.369	−2.369	4.000	5.952	6.369	2.369	4.369	2.000	0.500	0.658	**94.00**
			A	−57320.89	−6.373	−2.441	3.932	11.481	6.373	2.441	4.407	1.966	0.509	0.659	
Mt-3-PQPP	0.000275	303	G	−31560.33	−6.527	4.947	11.474	3.342	6.527	−4.947	0.790	5.737	0.174	0.541	**93.69**
			A	−31560.33	−6.527	4.947	11.474	3.342	6.527	−4.947	0.790	5.737	0.174	0.541	
Cl-4-PQPP	0.000275	303	G	−40855.49	−6.823	4.834	11.658	1.247	6.823	−4.834	0.995	5.829	0.172	0.515	**92.27**
			A	−40855.49	−6.823	4.834	11.658	1.247	6.823	−4.834	0.995	5.829	0.172	0.515	
QN1	0.005000	303	G	−32290.52	−5.591	−2.421	3.170	0.539	5.591	2.421	4.006	1.585	0.631	0.945	**93.00**
			A	−31687.93	−5.667	4.602	10.269	1.860	5.667	−4.602	0.533	5.135	0.195	0.630	
QN2	0.005000	303	G	−21756.03	−5.742	−2.606	3.136	2.513	5.742	2.606	4.174	1.568	0.638	0.901	**90.00**
			A	−21756.41	−5.845	−2.739	3.106	3.753	5.845	2.739	4.292	1.553	0.644	0.872	
QN3	0.005000	303	G	−24467.82	−5.714	4.585	10.299	1.733	5.714	−4.585	0.564	5.149	0.194	0.625	**87.00**
			A	−24467.82	−5.713	4.584	10.297	1.733	5.713	−4.584	0.565	5.149	0.194	0.625	
QN4	0.005000	303	G	−21408.61	−5.959	4.529	10.488	2.008	5.959	−4.529	0.715	5.244	0.191	0.599	**85.00**
			A	−21408.61	−5.959	4.530	10.489	2.008	5.959	−4.530	0.715	5.244	0.191	0.599	
Pr-N-Q = O	0.001000	303	G	−17304.46	−6.355	5.263	11.618	2.056	6.355	−5.263	0.546	5.809	0.172	0.555	**88.80**
			A	−17634.00	−6.593	−2.226	4.367	4.608	6.593	2.226	4.410	2.184	0.458	0.593	
Pr-N-Q = S	0.001000	303	G	−26421.81	−6.044	−2.555	3.488	4.015	6.044	2.555	4.299	1.744	0.573	0.774	**92.30**
			A	−26422.09	−6.292	−2.680	3.612	6.436	6.292	2.680	4.486	1.806	0.554	0.696	
QX	0.001000	298	G	−11374.34	−6.987	−2.299	4.688	0.596	6.987	2.299	4.643	2.344	0.427	0.503	**84.20**
			A	−11374.52	−7.031	−2.382	4.649	0.765	7.031	2.382	4.706	2.325	0.430	0.493	

Table 3 (*continued*)

Quinoxalines	Conc* (M)	Temp* (K)	Phase	TE (eV)	E_{HOMO} (eV)	E_{LUMO} (eV)	ΔE (eV)	μ (D)	IP (eV)	EA (eV)	X (eV)	η (eV)	σ (eV⁻¹)	ΔN	IE%*
CHQX	0.001000	298	G	−23880.88	−7.184	−2.533	4.651	2.399	7.184	2.533	4.859	2.325	0.430	0.460	**92.50**
			A	−23881.05	−7.144	−2.554	4.590	3.161	7.144	2.554	4.849	2.295	0.436	0.469	
THQX	0.001000	298	G	−22209.92	−6.620	−2.326	4.295	1.087	6.620	2.326	4.473	2.147	0.466	0.588	**95.50**
			A	−22210.15	−6.659	−2.386	4.273	1.422	6.659	2.386	4.522	2.136	0.468	0.580	
PHQX	0.001000	298	G	−19709.40	−6.187	−2.240	3.947	1.951	6.187	2.240	4.214	1.974	0.507	0.706	**98.30**
			A	−19709.72	−6.263	−2.386	3.877	2.435	6.263	2.386	4.325	1.938	0.516	0.690	
Q = O	0.001000	308	G	−14492.12	−6.538	−2.117	4.421	3.335	6.538	2.117	4.328	2.210	0.452	0.604	**66.60**
			A	−14492.44	−6.553	−2.168	4.384	4.846	6.553	2.168	4.360	2.192	0.456	0.602	
Q = S	0.001000	308	G	−23280.35	−6.115	−2.573	3.541	4.192	6.115	2.573	4.344	1.771	0.565	0.750	**82.80**
			A	−23280.66	−6.271	−2.649	3.622	6.751	6.271	2.649	4.460	1.811	0.552	0.701	
Cl-Q = S	0.001000	308	G	−35786.78	−6.275	−2.759	3.516	2.501	6.275	2.759	4.517	1.758	0.569	0.706	**75.00**
			A	−35787.08	−6.355	−2.747	3.609	4.469	6.355	2.747	4.551	1.804	0.554	0.679	
CMOPTQ	0.010000	303	G	−45481.52	−6.199	4.034	10.233	4.906	6.199	−4.034	1.082	5.116	0.195	0.578	**89.00**
			A	−45481.52	−6.199	4.034	10.233	4.906	6.199	−4.034	1.082	5.116	0.195	0.578	
CMOSQ	0.010000	303	G	−36822.14	−5.919	4.236	10.156	1.767	5.919	−4.236	0.842	5.078	0.197	0.606	**87.00**
			A	−37439.97	−5.805	−2.731	3.074	1.689	5.805	2.731	4.268	1.537	0.651	0.889	
MOSMQ	0.000100	298	G	−25517.79	−5.633	4.640	10.274	2.138	5.633	−4.640	0.496	5.137	0.195	0.633	**92.00**
			A	−25517.79	−5.633	4.640	10.274	2.138	5.633	−4.640	0.496	5.137	0.195	0.633	
FVQ	0.000100	298	G	−21756.03	−5.742	−2.606	3.136	2.513	5.742	2.606	4.174	1.568	0.638	0.901	**94.00**
			A	−21756.41	−5.845	−2.739	3.106	3.753	5.845	2.739	4.292	1.553	0.644	0.872	
DMQ = O	0.000100	298	G	−15271.34	−6.267	5.384	11.651	2.631	6.267	−5.384	0.441	5.825	0.172	0.563	**88.07**
			A	−15271.34	−6.267	5.384	11.651	2.631	6.267	−5.384	0.441	5.825	0.172	0.563	
DMQ = S	0.010000	298	G	−23960.66	−5.348	4.890	10.239	2.871	5.348	−4.890	0.229	5.119	0.195	0.661	**93.27**
			A	−23960.66	−5.348	4.890	10.238	2.871	5.348	−4.890	0.229	5.119	0.195	0.661	
Q-HNHyQ	0.001000	298	G	−42704.01	−6.235	5.150	11.384	3.496	6.235	−5.150	0.542	5.692	0.176	0.567	**89.40**
			A	−42704.01	−6.235	5.150	11.384	3.496	6.235	−5.150	0.542	5.692	0.176	0.567	
Q-CH3NHyQ	0.001000	298	G	−44583.73	−6.081	−2.033	4.047	6.401	6.081	2.033	4.057	2.024	0.494	0.727	**95.40**
			A	−43753.97	−6.172	5.158	11.329	3.774	6.172	−5.158	0.507	5.665	0.177	0.573	
HQ	0.001000	303	G	−42072.41	−5.323	5.519	10.842	1.961	5.323	−5.519	−0.098	5.421	0.184	0.655	**91.00**
			A	−42707.73	−4.741	−1.263	3.478	2.418	4.741	1.263	3.002	1.739	0.575	1.149	
CQ	0.001000	303	G	−43777.44	−4.566	−1.266	3.300	2.024	4.566	1.266	2.916	1.650	0.606	1.238	**94.20**
			A	−43122.36	−5.251	5.541	10.793	2.131	5.251	−5.541	−0.145	5.396	0.185	0.662	
CSQN	0.001000	303	G	−33762.98	−6.162	4.271	10.433	4.983	6.162	−4.271	0.946	5.217	0.192	0.580	**92.80**
			A	−33762.98	−6.162	4.271	10.433	4.984	6.162	−4.271	0.946	5.217	0.192	0.580	
NSQN	0.001000	303	G	−24986.21	−5.445	4.659	10.104	1.236	5.445	−4.659	0.393	5.052	0.198	0.654	**96.40**
			A	−24986.21	−5.445	4.659	10.104	1.236	5.445	−4.659	0.393	5.052	0.198	0.654	

* Experimental parameters i.e temperature, concentration and experimental IE% were retrieved from published studies.
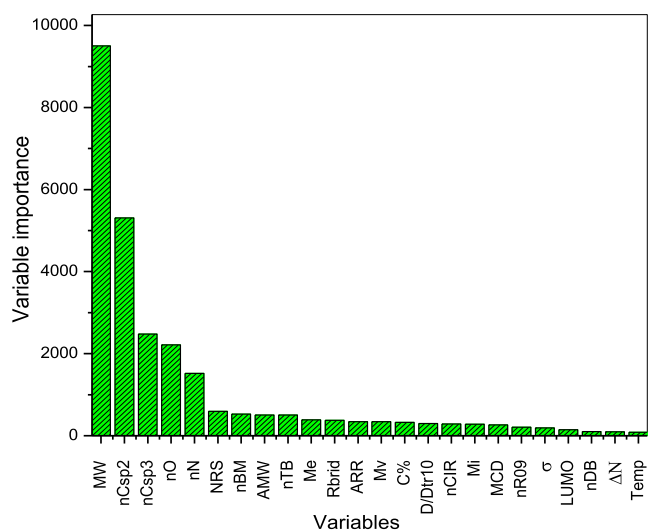
Fig. 2 Significance of molecular descriptors to the inhibition efficiencies of quinoxalines.

Table 4 Definition of the selected descriptors for model building.

Descriptors	Group name	Description
MW	Constitutional indices	Molecular weight
nN	Constitutional indices	Number of nitrogen atoms
nO	Constitutional indices	Number of oxygen atoms
nCsp3	Constitutional indices	Number of sp^3 hybridized carbon atoms
nCsp2	Constitutional indices	Number of sp^2 hybridized carbon atoms

sites for molecular adherence on the metallic substrate ((Lgaz et al., 2016a; Olasunkanmi et al., 2016a) Benhiba et al., 2020, Olasunkanmi and Ebenso, 2020).

Table 6 presents the ANOVA and regression coefficients table, which shows a p-value slightly higher than expected. It is clear that the model lacks the capability to accurately explain the inhibition mechanism of quinoxalines on the account of its low R^2, high SD and high sum of squares error (SSE). Thus, it is mandatory to employ a nonlinear model to further investigate the relationship between the screened variables and the IE% of quinoxaline-based corrosion inhibitors.

Table 6 Analysis of variance and regression coefficients for the OLS model.

Source	DF	Adj SS	Adj MS	F-value	p-value
Regression	6	745.92	124.320	2.37	0.052
Conc	1	15.58	15.578	0.30	0.590
MW	1	37.94	37.942	0.72	0.401
nN	1	127.18	127.180	2.42	0.129
nO	1	67.97	67.969	1.29	0.263
nCsp3	1	649.92	649.924	12.38	0.001
nCsp2	1	4.06	4.056	0.08	0.783
Error	33	1732.68	52.506		
Lack-of-Fit	28	1725.83	61.637	44.97	0.000
Pure Error	5	6.85	1.371		
Total	39	2478.60			

| Term	Coeff	SE Coeff	T-value	p-value
Constant	74.84	5.860	12.77	0.000
Conc	270.00	496.000	0.54	0.590
MW	0.04	0.052	0.85	0.401
nN	4.92	3.160	1.56	0.129
nO	−1.89	1.660	−1.14	0.263
nCsp3	−4.00	1.140	−3.52	0.001
nCsp2	−0.17	0.613	−0.28	0.783

3.4. ANN model: internal validation

The inadequacy of the proposed linear model mandated the development of a nonlinear model to better comprehend the relationship between the descriptors and the IE% for quinoxaline compounds studied as anticorrosive agents. The neural network models were established to model the connection between the experimental IE% and the predicted IE%. The internal validation was carried out using k-fold validation technique. A k-fold of 5 was used which implies that the quinoxaline dataset was randomly divided into five equal groups and four groups (i.e., 32 compounds) were used to train the model in each case and one group (i.e., 8 compounds) was utilized to check the accuracy of the established model.

The results of the training and validation phase of the ANN built models for quinoxaline inhibitors are displayed in Fig. 3. The plots show instances of the calculated IE% diverging from the measured IE%. These divergences are observed both at the training and validation phases of the model development process. At the training phase, models 1 and 2 showed clear cases of underprediction while model 5 was clearly overpredicting the measured IE%. Models 3 and 4 revealed fair cases of divergence. At the validation stage, models 2, 4 and 5 clearly underpredict the checking dataset, while model 3 is a case of

Table 5 Correlation matrix of selected features.

	Conc	MW	nN	nO	nCsp3	nCsp2	IE%
Conc	1	−0.224	−0.473	−0.123	−0.427	−0.018	0.103
MW	−0.224	1	0.845	0.819	0.697	0.818	0.108
nN	−0.473	0.845	1	0.709	0.849	0.482	0.023
nO	−0.123	0.819	0.709	1	0.504	0.629	0.079
nCsp3	−0.427	0.697	0.849	0.504	1	0.341	−0.246
nCsp2	−0.018	0.818	0.482	0.629	0.341	1	0.165
IE%	0.103	0.108	0.023	0.079	−0.246	0.165	1
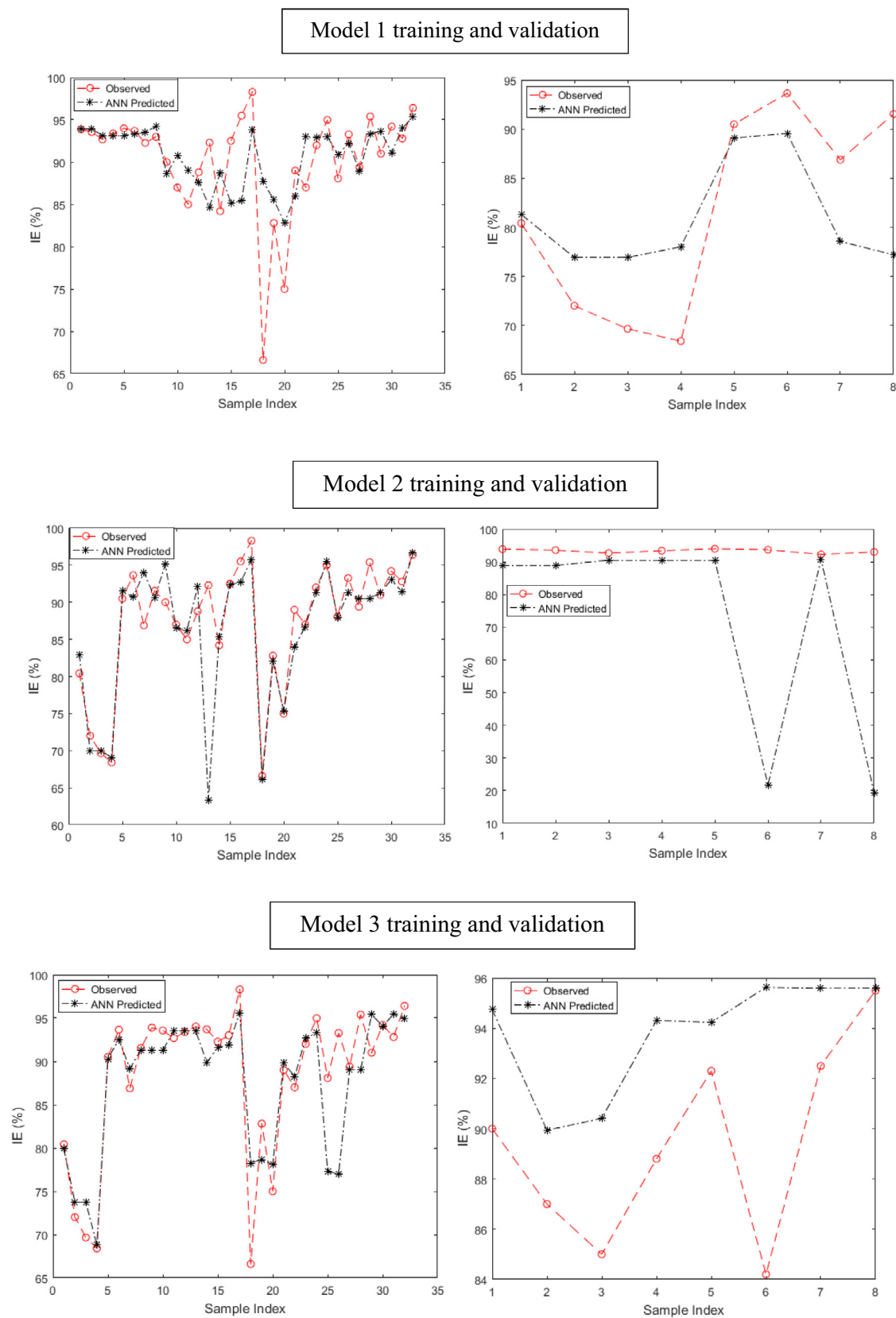
Fig. 3 Experimental IE% and predicted IE% at the model training and validation phase for quinoxaline derivatives (models 1–5).

Model 4 training and validation
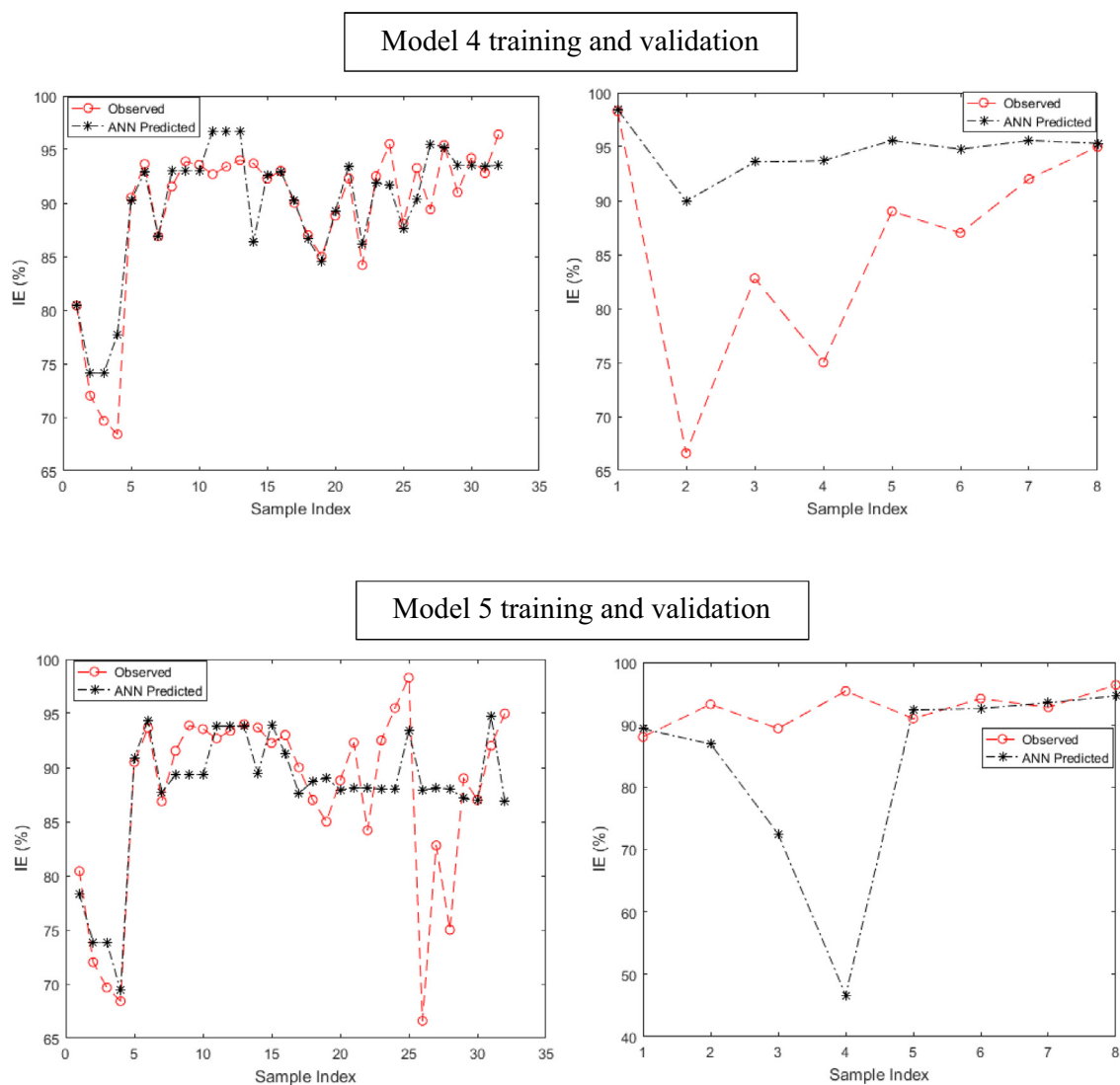

Model 5 training and validation

Fig. 3 (*continued*)

overprediction. These observed discrepancies between the experimental and calculated IE% are attributed to the misfiring of the neural network node (Adedeji et al., 2019).

ANN architecture used for model development was reported on Table 7 as 6-3-5-1. This implies that six molecular variables were used as input variables with 3 and 5 neurons at the hidden layers and an output of IE%. The error estimates between the measured and the predicted IE% have been established to be a reliable means of assessing the ability of the proposed models. Several statistical performance indices have been employed in this work to appraise the reliability and predictive power of the developed models. These include error functions such as MSE, RMSE, MAD and MAPE. These have been reported in other fields as excellent metrics to evaluate neural network models (Aouidate et al., 2016, Abdel-Ilah et al., 2017, Eftekhari et al., 2018). The selection of the best model is achieved by considering the model that yields the lowest values of these error functions and also shows minor variance between the training and val-

idation phase (Gramatica, 2013). On this basis, the five proposed models with their respective error functions have been displayed in Table 7.

A careful comparison of the presented data in the table shows that model 3 could be adjudged to be the least biased to the selected dataset, based on statistical error analyses tools. This is because model 3 is characterized by consistent lower values of MSE, RMSE, MAD and MAPE when compared to the other developed models. Models 1 and 4 showed some promising error functions at some levels but were inconsistent with large variance between the training and validation phase.

3.5. ANN model: external validation

From the above findings and using the variants of molecules that yielded the highest inhibition efficiencies from experimental assessments, ten new quinoxaline compounds were theoretically designed. The inhibition performances of these novel quinoxalines were assessed using the QSPR models developed

Table 7 ANN predictive model performance at the training and validation phase.

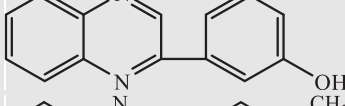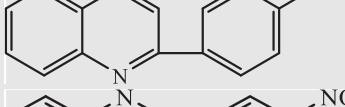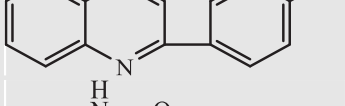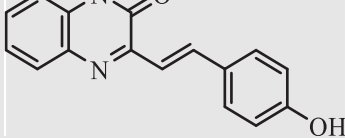| Metric	Model 1		Model 2		Model 3		Model 4		Model 5		Average	
	Train	Validation	Train	Validation	Train	Validation	Train	Validation	Train	Validation	Train	Validation
MSE	27.7813	57.9311	32.1215	1304.0	21.2783	29.3336	8.9254	140.9121	30.7511	338.9934	24.1715	380.4940
RMSE	5.2708	7.6112	5.6676	36.5421	4.6128	5.4160	2.9875	11.8706	5.5454	18.4118	4.8168	15.9703
MAD	3.3810	6.3525	2.7213	26.0772	2.8527	2.3816	2.0521	6.5330	3.6843	11.9122	2.9383	10.6513
MAPE	4.0055	7.9444	2.8803	22.1418	3.3460	5.0389	2.3188	11.7086	4.4810	10.5053	3.4063	11.4678
rMBE	0.5134	−0.8351	−1.1694	−22.1535	−0.8127	4.9120	0.6472	10.3818	0.3852	−9.7155	−2.1074	−3.4821
CoV	0.0171	0.0174	0.0440	0.0091	0.0296	0.0112	0.27	0.0098	0.0138	0.0357	0.1503	0.0166
Iterations	141		245		64		620		471		−	
Topology	6-3-5-1		6-3-5-1		6-3-5-1		6-3-5-1		6-3-5-1		6-3-5-1	
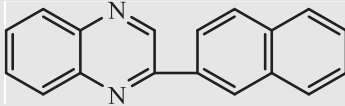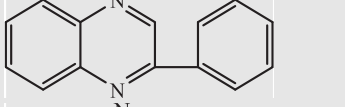
Table 8 Descriptors for novel quinoxaline molecules.

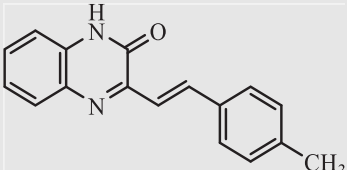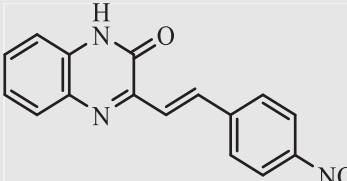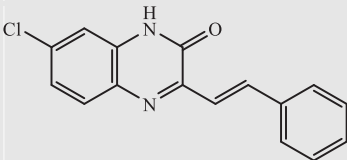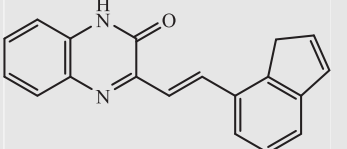| Compounds	Conc	MW	nN	nO	nCsp3	nCsp2
A	0.001	256.32	2	0	0	18
B	0.001	206.26	2	0	0	14
C	0.001	222.26	2	1	0	14
D	0.001	220.29	2	0	1	14
E	0.001	251.26	3	2	0	14
F	0.001	264.30	2	2	0	16
G	0.001	262.33	2	1	1	16
H	0.001	293.30	3	3	0	16
I	0.001	282.74	2	1	0	16
J	0.001	286.35	2	1	1	18

from MLR and ANN techniques. The calculated descriptors of the novel quinoxalines obtained from Dragon 7.0 software are displayed in Table 8.

The chemical names and structures of the novel quinoxalines proposed as efficient anticorrosive agents for mild steel deterioration in HCl at 0.001 M are presented on Table 9. The predicted inhibition performances ranged from 87.88 to 94.77% for MLR model and 94.59 to 95.73% for the ANN model. The predicted IE% from the developed MLR and ANN models show that the novel quinoxalines are excellent inhibitors of acidic corrosion. The effect of the presence of substituents on the IE% of the newly designed quinoxaline molecules are also observed as is often reported in literature

Table 9 Inhibition efficiencies of novel quinoxaline molecules from MLR and ANN models.

Quinoxalines	IUPAC nomenclature	Molecular structure	MLR predicted IE%	ANN predicted IE%
A.	2-phenylquinoxaline		93.17	94.80
B.	2-(naphthalen-2-yl)quinoxaline		91.65	95.65
C.	3-(quinoxalin-2-yl)phenol		90.46	95.60
D.	2-(p-tolyl)quinoxaline		88.26	95.21
E.	2-(4-nitrophenyl)quinoxaline		94.77	95.73
F.	(E)-3-(4-hydroxystyryl)quinoxalin-2(1H)-one		90.08	95.60

Table 9 (continued)

Quinoxalines	IUPAC nomenclature	Molecular structure	MLR predicted IE%	ANN predicted IE%
G.	(E)-3-(4-methylstyryl)quinoxalin-2(1H)-one		87.88	95.27
H.	(E)-3-(4-nitrostyryl)quinoxalin-2(1H)-one		94.39	95.66
I.	(E)-7-chloro-3-styrylquinoxalin-2(1H)-one		92.78	95.46
J.	(E)-3-(2-(1H-inden-7-yl)vinyl)quinoxalin-2(1H)-one		88.60	94.59
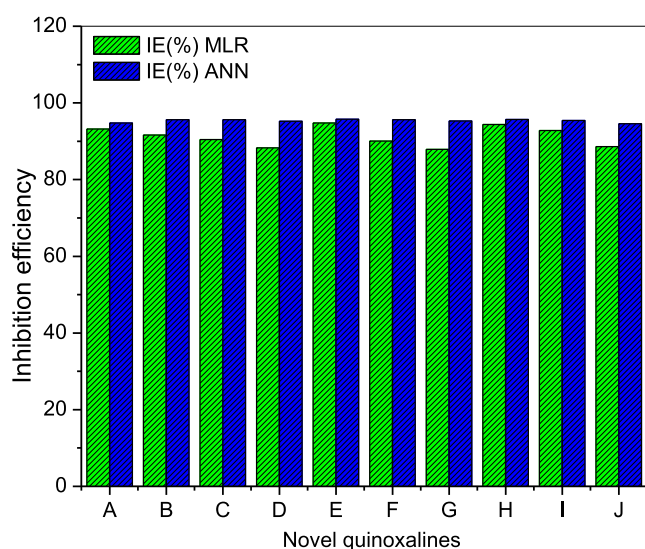
Fig. 4 Comparison of predicted IE% of novel quinoxalines obtained with MLR and ANN models.

(Fu et al., 2012 (Lgaz et al., 2016b) Tazouti et al., 2016, Benhiba et al., 2020).

Fig. 4 showed a graphical representation of the predicted IE % from MLR and ANN models. It is obvious from the plot that the best ANN model showed a better surface coverage of the novel quinoxaline-based inhibitors on the mild steel surface in molar HCl than the linear model.

A statistical analysis to ascertain whether the difference between the MLR and ANN models for the inhibition performance of the novel quinoxalines is statistically significant was conducted and the outcome is presented in Table 10. At a confidence level of 0.05, F (26.31093) > F_{crit} (4.413873) which shows that there is a statistically significant variance between the MLR and ANN models for the test dataset.

4. Conclusions

1. Quantum chemical studies of 40 quinoxalines was performed and the orbital density distribution images provided information on the probable sites of adsorption. Molecular descriptors were calculated using DFT method and Dragon 7 software.

Table 10 Analysis of variance between the MLR and ANN predicted test results.

Source of variation	SS	df	MS	F	p-value	F_{crit}
Between Groups	86.22407	1	86.22407	26.31093	7.02E-05	4.413873
Within Groups	58.98817	18	3.27712			
Total	145.2122	19				

2. Linear model showed poor correlation with the experimental IE% and high statistical error values which portends that corrosion inhibition mechanism is a complex nonlinear process that is affected by many factors. Nonlinear neural network presented a more reliable and robust alternative to modelling inhibition data to gain insight into inhibition mechanism.

3. The established models suggest that the considered constitutional indices comprising molecular weight, number of oxygen atoms, number of nitrogen atoms and number of hybridized carbon atoms form an efficient group of molecular descriptors for QSPR modelling of quinoxaline inhibitors. Thus, constitutional indices are crucial for determining the inhibition efficiencies of quinoxaline molecules.

4. Excellent inhibition performances of the 10 novel quinoxaline-based inhibitors obtained from the forecast using the developed QSPR models suggest that the non-synthesized compounds are potential organic compounds that can be explored experimentally as safe and effective inhibitors of metallic deterioration in molar HCl.

CRediT authorship contribution statement

Taiwo W. Quadri: Investigation, Data curation, Writing-Original draft. **Lukman O. Olasunkanmi:** Investigation, Data curation, Writing-Original draft. **Omolola E. Fayemi:** Investigation, Data curation, Writing-Original draft. **Hassane Lgaz:** Methodology, Validation, Formal analysis, Writing - Review & Editing, Supervision, Funding acquisition. **Omar Dagdag:** Investigation, Data Curation, Software, Writing - Review & Editing. **El-Sayed M. Sherif:** Investigation, Data Curation, Software, Writing - Review & Editing. **Awad A. Alrashdi:** Methodology, Validation, Formal analysis, Writing - Review & Editing, Supervision, Funding acquisition. **Ekemini D. Akpan:** Investigation, Data Curation, Software, Writing - Review & Editing. **Han-Seung Lee:** Methodology, Validation, Formal analysis, Writing - Review & Editing, Supervision, Funding acquisition. **Eno E. Ebenso:** Methodology, Validation, Formal analysis, Writing - Review & Editing, Supervision, Funding acquisition.

Declaration of Competing Interest

The authors declare that they have no known competing financial interests or personal relationships that could have appeared to influence the work reported in this paper.

Acknowledgements

References

Abdel-Ilah, L.E., Veljović , G.L., et al., 2017. Applications of QSAR study in drug design Int. J. Eng. Res. Tech. 6, 582–587.

Adardour, K., Kassou, O., Touir, R., et al, 2010. Study of the influence of new quinoxaline derivatives on corrosion inhibition of mild steel in hydrochloric acidic medium. J. Mater. Environ. Sci. 1, 129–138.

Adardour, K., Touir, R., Ramli, Y., et al, 2013. Comparative inhibition study of mild steel corrosion in hydrochloric acid by new class synthesised quinoxaline derivatives: part I. Res. Chem. Intermed. 39, 1843–1855. https://doi.org/10.1007/s11164-012-0719-2.

Adedeji, P.A., Akinlabi, S., Madushele, N., et al, 2019. Neuro-fuzzy mid-term forecasting of electricity consumption using meteorological data. IOP Conference Series: Earth and Environmental Science. IOP Publishing.

Adedeji, P.A., Akinlabi, S., Madushele, N., et al, 2020a. Wind turbine power output very short-term forecast: a comparative study of data clustering techniques in a PSO-ANFIS model. J. Clean. Prod. 254, 120135.

Adedeji, P.A., Akinlabi, S.A., Madushele, N., et al, 2020b. Neuro-fuzzy resource forecast in site suitability assessment for wind and solar energy: a mini review. J. Clean. Prod. 122104.

Al-Fakih, A.M., Algamal, Z.Y., Lee, M.H., et al, 2016. Quantitative structure–activity relationship model for prediction study of corrosion inhibition efficiency using two-stage sparse multiple linear regression. J. Chemom. 30, 361–368. https://doi.org/10.1002/cem.2800.

Aouidate, A., Ghaleb, A., Ghamali, M., et al, 2016. Combining DFT and QSAR studies for predicting psychotomimetic activity of substituted phenethylamines using statistical methods. J. Taibah Univ. Sci. 10, 787–796.

Benbouya, K., Zerga, B., Sfaira, M., et al, 2012. WL, IE and EIS studies on the corrosion behaviour of mild steel by 7-substituted 3-methylquinoxalin-2 (1H)-ones and thiones in hydrochloric Acid medium. Int. J. Electrochem. Sci. 7, 6313–6330.

Benhiba, F., Benzekri, Z., Guenbour, A., et al, 2020. Combined electronic/atomic level computational, surface (SEM/EDS), chemical and electrochemical studies of the mild steel surface by quinoxalines derivatives anti-corrosion properties in 1 molͦ L-1 HCl solution. Chin. J. Chem. Eng., 1436–1458

Chauhan, D.S., Singh, P., Quraishi, M., 2020. Quinoxaline derivatives as efficient corrosion inhibitors: current status, challenges and future perspectives. J. Mol. Liq., 114387

Eftekhari, M., Yadollahi, A., Ahmadi, H., et al, 2018. Development of an artificial neural network as a tool for predicting the targeted phenolic profile of grapevine (Vitis vinifera) foliar wastes. Front. Plant Sci. 9, 837–846.

El-Hajjaji, F., Zerga, B., Sfaira, M., et al, 2014. Comparative study of novel N-substituted quinoxaline derivatives towards mild steel corrosion in hydrochloric acid: part 1. J. Mater. Environ. Sci. 5, 255–262.

Fu, J., Zang, H., Wang, Y., et al, 2012. Experimental and theoretical study on the inhibition performances of quinoxaline and its derivatives for the corrosion of mild steel in hydrochloric acid. Ind. Eng. Chem. Res. 51, 6377–6386.

Golbraikh, A., Wang, X.S., Zhu, H., et al, 2012. Predictive QSAR Modeling: Methods and Applications in Drug Discovery and Chemical Risk Assessment. Handbook of computational chemistry, Springer, Netherlands, pp. 1309–1342.

Goni, L., Mazumder, M.A. 2019. Green corrosion inhibitors. Corrosion Inhibitors, IntechOpen.

Gramatica, P., 2013. On the Development and Validation of QSAR models. Computational Toxicology, Springer: 499–526.

Khaled, K.F., Al-Mobarak, N.A., 2012. A predictive model for corrosion inhibition of mild steel by thiophene and its derivatives using artificial neural network. Int. J. Electrochem. Sci. 7, 1045–1059.

Khan, A.U., 2016. Descriptors and their selection methods in QSAR analysis: paradigm for drug design. Drug Discovery Today. 21, 1291–1302.

Kokalj, A., 2010. Is the analysis of molecular electronic structure of corrosion inhibitors sufficient to predict the trend of their inhibition performance. Electrochim. Acta 56, 745–755. https://doi.org/10.1016/j.electacta.2010.09.065.

Kokalj, A., 2021. On the alleged importance of the molecular electron-donating ability and the HOMO–LUMO gap in corrosion inhibition studies. Corros. Sci. 180, 109016.

Kokalj, A., Lozinšek, M., Kapun, B., et al, 2021. Simplistic correlations between molecular electronic properties and inhibition efficiencies: do they really exist? Corros. Sci. 179, 108856.

Laabaissi, T., Benhiba, F., Missioui, M., et al, 2020. Coupling of chemical, electrochemical and theoretical approach to study the corrosion inhibition of mild steel by new quinoxaline compounds in 1 M HCl. Heliyon. 6, e03939.

Lgaz, H., Saadouni, M., Salghi, R., et al, 2016a. A thermodynamical and electrochemical investigation of quinoxaline derivatives as corrosion inhibitors for mild steel in 1 M hydrochloric acid solution. Der Pharma Lett.

Lgaz, H., Salghi, R., Jodeh, S., et al, 2016b. Understanding the adsorption of quinoxaline derivatives as corrosion inhibitors for mild steel in acidic medium: Experimental, theoretical and molecular dynamic simulation studies. J. Steel Struct. Constr. 2, 1–17.

Li, L., Zhang, X., Gong, S., et al, 2015. The discussion of descriptors for the QSAR model and molecular dynamics simulation of benzimidazole derivatives as corrosion inhibitors. Corros. Sci. 99, 76–88. https://doi.org/10.1016/j.corsci.2015.06.003.

Lin, X., Li, X., Lin, X., 2020. A review on applications of computational methods in drug screening and design. Molecules 25, 1375.

Liu, Y., Guo, Y., Wu, W., et al, 2019. A machine learning-based QSAR model for benzimidazole derivatives as corrosion Inhibitors by incorporating comprehensive feature selection. Interdiscip. Sci. 11, 738–747.

Liu, Y., Zhao, T., Ju, W., et al, 2017. Materials discovery and design using machine learning. J. Materiomics. 3, 159–177. https://doi.org/10.1016/j.jmat.2017.08.002.

Mauri, A., Consonni, V., Pavan, M., et al, 2006. Dragon software: an easy approach to molecular descriptor calculations. Match 56, 237–248.

Mishra, A., Verma, C., Srivastava, V., et al., 2018. Chemical, electrochemical and computational studies of newly synthesized novel and environmental friendly heterocyclic compounds as corrosion inhibitors for mild steel in acidic medium. 4, 32.

O'Boyle, N.M., Banck, M., James, C.A., et al, 2011. Open Babel: An open chemical toolbox. J. Chemom. 3, 33.

Olasunkanmi, L.O., Ebenso, E.E., 2020. Experimental and computational studies on propanone derivatives of quinoxalin-6-yl-4, 5-dihydropyrazole as inhibitors of mild steel corrosion in hydrochloric acid. J. Colloid Interface Sci. 561, 104–116.

Olasunkanmi, L.O., Kabanda, M.M., Ebenso, E.E., 2016a. Quinoxaline derivatives as corrosion inhibitors for mild steel in hydrochloric acid medium: electrochemical and quantum chemical studies. Physica E Low Dimens. Syst. Nanostruct. 76, 109–126.

Olasunkanmi, L.O., Obot, I.B., Ebenso, E.E., 2016b. Adsorption and corrosion inhibition properties of N-{n-[1-R-5-(quinoxalin-6-yl)-4, 5-dihydropyrazol-3-yl] phenyl} methanesulfonamides on mild steel in 1 M HCl: experimental and theoretical studies. RSC Adv. 6, 86782–86797.

Olasunkanmi, L.O., Obot, I.B., Kabanda, M.M., et al, 2015. Some quinoxalin-6-yl derivatives as corrosion inhibitors for mild steel in hydrochloric acid: experimental and theoretical studies. J. Phys. Chem. C 119, 16004–16019.

Olatunji, O.O., Akinlabi, S., Madushele, N., et al, 2019. Estimation of the elemental composition of biomass using hybrid adaptive neuro-fuzzy inference system. BioEnergy Res. 12, 642–652.

Ouakki, M., Galai, M., Benzekri, Z., et al, 2021. Insights into corrosion inhibition mechanism of mild steel in 1 M HCl solution by quinoxaline derivatives: electrochemical, SEM/EDAX, UV-visible, FT-IR and theoretical approaches. Colloids Surf. A: Physicochem. Eng. Aspects 611, 125810.

Puzyn, T., Leszczynski, J., Cronin, M.T., 2010. Recent Advances in QSAR Studies: Methods and Applications. Springer Science & Business Media.

Quadri, T.W., Olasunkanmi, L.O., Akpan, E.D., et al, 2021a. Chromeno-carbonitriles as corrosion inhibitors for mild steel in acidic solution: electrochemical, surface and computational studies. RSC Adv. 11, 2462–2475.

Quadri, T.W., Olasunkanmi, L.O., Fayemi, O.E., et al, 2021b. Quantitative structure activity relationship and artificial neural network as vital tools in predicting coordination capabilities of organic compounds with metal surface: A review. Coord. Chem. Rev. 446, 214101.

Rbaa, M., Galai, M., El Faydy, M., et al, 2018. Synthesis and characterization of new quinoxaline derivatives of 8-hydroxyquinoline as corrosion inhibitors for mild steel in 1.0 M HCl medium. J. Mater. Environ. Sci. 9, 172–188.

Roy, K., Kar, S., Das, R.N., 2015a. A Primer on QSAR/QSPR Modeling: Fundamental Concepts. Springer.

Roy, K., Kar, S., Das, R.N., 2015b. Understanding the Basics of QSAR for Applications in Pharmaceutical Sciences and Risk Assessment. Academic press.

Rybińska-Fryca, A., Sosnowska, A., Puzyn, T., 2020. Representation of the structure—a key point of building QSAR/QSPR models for ionic liquids. Materials 13, 2500.

Saranya, J., Lavanya, K., Kiranmai, M.H., et al, 2021. Quinoxaline derivatives as anticorrosion additives for metals. Corros. Rev. 39, 79–92.

Tazouti, A., Galai, M., Touir, R., et al, 2016. Experimental and theoretical studies for mild steel corrosion inhibition in 1.0 M HCl by three new quinoxalinone derivatives. J. Mol. Liq. 221, 815–832.

Topliss, J.G., Costello, R.J., 1972. Chance correlations in structure-activity studies using multiple regression analysis. J. Med. Chem. 15, 1066–1068.

Topliss, J.G., Edwards, R.P., 1979. Chance factors in studies of quantitative structure-activity relationships. J. Med. Chem. 22, 1238–1244.

Winkler, D., Breedon, M., White, P., et al, 2016. Using high throughput experimental data and in silico models to discover alternatives to toxic chromate corrosion inhibitors. Corros. Sci. 106, 229–235.

Winkler, D.A., Breedon, M., Hughes, A.E., et al, 2014. Towards chromate-free corrosion inhibitors: structure–property models for organic alternatives. Green Chem. 16, 3349–3357. https://doi.org/10.1039/C3GC42540A.

Yusuf, T.L., Quadri, T.W., Tolufashe, G.F., et al, 2020. Synthesis and structures of divalent Co, Ni, Zn and Cd complexes of mixed dichalcogen and dipnictogen ligands with corrosion inhibition properties: experimental and computational studies. RSC Adv. 10, 41967–41982.

Zarrouk, A., El Ouali, I., Bouachrine, M., et al, 2013. Theoretical approach to the corrosion inhibition efficiency of some quinoxaline derivatives of steel in acid media using the DFT method. Res. Chem. Intermed. 39, 1125–1133.

Zarrouk, A., Hammouti, B., Dafali, A., et al, 2014. A theoretical study on the inhibition efficiencies of some quinoxalines as corrosion inhibitors of copper in nitric acid. J. Saudi Chem. Soc. 18, 450–455. https://doi.org/10.1016/j.jscs.2011.09.011.

Zhao, H., Zhang, X., Ji, L., et al, 2014. Quantitative structure–activity relationship model for amino acids as corrosion inhibitors based on the support vector machine and molecular design. Corros. Sci. 83, 261–271. https://doi.org/10.1016/j.corsci.2014.02.023.